BUBBLE SIZING BY THE NONLINEAR SCATTERING OF TWO ACOUSTIC FREQUENCIES

T. G. LEIGHTON, R. J. LINGARD, A. J. WALTON, J. E. FIELD
Cavendish Laboratory,
Madingley Road,
Cambridge CB3 OHE
UK

ABSTRACT If two acoustic frequencies (ω_p and ω_i) are incident upon a bubble, and if one of those (ω_p, the 'pump' frequency) corresponds to the bubble resonance, the sum and difference frequencies ($\omega_i \pm \omega_p$) may be scattered. The detection of these has, in the past, been used to indicate the bubble size. In this experiment, the resonance response curve for the scattering of the sum and difference frequencies has been studied, to investigate the uncertainty inherent in their use as bubble sizing tools. These response curves were then compared with those of the sub-sum ($\omega_i+\frac{1}{2}\omega_p$) and sub-difference ($\omega_i-\frac{1}{2}\omega_p$) frequencies. It was found that the sub-sum and sub-difference resonance curves are often of smaller width than those due to the corresponding sum- and difference-frequencies. The sub-sum and sub-difference frequencies therefore demonstrate greater potential for accurate bubble sizing. The scattered frequencies were used to acoustically resolve known bubble arrays.

1. Introduction

When a gas bubble in a liquid is insonified, it may undergo volume pulsations. One of the commonest equations that describe the response of a single isolated bubble (of radius R, and equilibrium radius R_0) to a time-varying pressure is the Rayleigh-Plesset (or RPNNP) equation:

$$R\ddot{R} + 3\dot{R}^2/2 = (1/\rho)\{(P_0 + 2\sigma/R_0 - P_v)(R_0/R)^{3\kappa} - 2\sigma/R - 4\mu\dot{R}/R - P_0 - P(t)\}, \quad (1)$$

where σ, ρ and μ are respectively the surface tension, density and viscosity of the liquid; P_0 the hydrostatic pressure, and P(t) the time-varying pressure component (ie. the forcing term). P_v is the vapour pressure within the bubble, and κ the polytropic index of the gas (which takes values between 1 and γ, the ratio of the specific heats at constant pressure and volume, depending on whether the gas behaves isothermally, adiabatically, or in some intermediate manner). When the surface tension and viscosity terms in the Rayleigh-Plesset equation are deemed negligible, and P(t) set to zero, the formulation approximates to the simple harmonic oscillations of an unforced bubble, with resonance frequency given by

$$\nu_r = (1/2\pi R_0).\sqrt{(3\kappa P_0/\rho)}\ , \quad (2)$$

B. R. Kerman (ed.), Natural Physical Sources of Underwater Sound, 453–466.

A simple derivation of this equation is given by Minnaert (1933). For air bubbles in water under one atmosphere, equation 2 reduces to

$$\nu_r \cdot R_0 \approx 3 \text{ Hz.m} \quad . \tag{3}$$

The acoustic output of such a freely-oscillating bubble is typically an exponentially-decaying sinusoid, which has been recorded in the sound of many phenomena, including the babbling of brooks (Leighton and Walton, 1987) and the impact of water drops on a body of liquid; the "noise of a dripping tap" (Pumphrey and Walton, 1988; Pumphrey and Crum, 1989). Leighton and Walton (1987) used these natural oscillations to acoustically size bubbles in brookes.

The ability to elicit the presence and radius of bubbles (whether isolated or in clouds) has been the subject of much research owing to the wealth of application of the technique. There are applications in fluid processing (Neppiras, 1980), the measurement of pressure changes (Shankar et al., 1986). Medical applications include the study of decompression sickness (Belcher ,1980; and Kisman, 1977), and contrast echocardiography (Tickner, 1982). Hulshof and Schurink (1985) used the scattering of continuous-wave ultrasound to detect steam bubbles in high-pressure vessels; Gross et al. (1985) detected bubbles produced *in vivo* by ultrasound in a canine cardiovascular system, using an acoustic detection system of Miller et al. (1984). This Resonance Bubble Detector (RBD) detects the second harmonic when the resonant frequency impinges upon a bubble. The insonating frequency is fixed in the RBD, limiting the range of bubbles detectable. Watkins et al. (1988) scattered sound from bubbles in liquid sodium coolant to monitor the internal states of nuclear reactors.

Resonance excitation (Fairbank and Scully, 1977), Doppler techniques (Nishi, 1972), and the generation of the second harmonic (Miller, 1981) have all been used in attempts to detect and size bubbles. All have drawbacks (Shankar et al., 1986). With resonance excitation, a large bubble far from resonance size can generate a stronger signal than a smaller bubble at resonance. Doppler can only be used on moving bubbles, and may be unable to distinguish between a single large bubble and a cluster of smaller ones. Spatial resolution is poor with the second harmonic technique.

Newhouse and Shankar (1984) introduced a sizing technique whereby a bubble is insonified by two acoustic frequencies, and Shankar et al. (1986) used the scattering of the sum and difference components to measure fluid pressure changes by acoustically monitoring the resulting change in equilibrium bubble size. The source of the sum and difference frequencies can be seen from simple theory.

A bubble in a sound field is clearly a nonlinear oscillator (see equation 1), and for any such oscillator the displacement can be expressed as a power series of the driving force. For a bubble, this would be,

$$R(t) = a.P(t) + b.P^2(t) + c.\ P^3(t) + d.\ P^4(t) + \ldots \quad , \tag{4}$$

where a, b, c and d are constants (Main, 1984). If the driving force were a single-frequency, the acoustic pressure would be $P(t)=P_A \cos\omega t$. If this were substituted into equation 4, it can easily be seen how the second, third etc. harmonics arise, since

$$2\cos^2 \omega t = 1+\cos 2\omega t \quad , \tag{5}$$

$$4\cos^3 \omega t = \cos 3\omega t + 3\cos\omega t \quad . \tag{6}$$

However the driving force might consist of the sum of two coherent forces of different frequency, ie.

$$P(t) = P_1\cos\omega_1 t + P_2\cos\omega_2 t \ , \tag{7}$$

assuming $\omega_2>\omega_1$ Note that the presence of phase constants would not alter the result. After substituting equation 7 into equation 4, expansion of the quadratic component contains a term which can be expanded to generate the sum and difference frequencies:

$$2P_2P_1\cos\omega_1 t \ .\cos\omega_2 t = P_2P_1\{\cos(\omega_1+\omega_2)t \ + \cos(\omega_2-\omega_1)t \ \} \tag{8}$$

Experimentally, Shankar et al. (1986) insonated the bubble with one 'imaging' beam (fixed at a frequency of 2.25 MHz) and a second, 'pumping' beam. The pump frequency was scanned across the region where the bubble resonance could reasonably be expected to lie. When the imaging and pump frequencies are far from the bubble resonance, the bubble response is small and it approximates well to a linear oscillator. Thus no sum- and difference-frequencies are detected. When the pump frequency is close to the bubble resonance, the amplitude of the radial oscillations becomes large. The nonlinear character of the bubble predominates, and it scatters nonlinearly. Thus the frequency of the pump signal when the sum- and difference-frequencies are detected can be related to the bubble resonance, and therefore to the bubble size (for example, through equation 3). Shankar et al. (1986) measured the frequency of the detected sum component to find the bubble size, but direct measurement of the pump frequency is a precaution against any drift in the imaging frequency. (Since the latter frequency is about 100 to 1000 times the pump frequency, then a 1% accuracy in the pump measurement requires 0.01% to 0.001% stability in the imaging frequency.)

In this present study, the off-resonance response of bubbles to pump (ω_p) and imaging (ω_i) frequencies is measured to investigate the accuracy with which bubbles can be sized. The resolution is compared with that obtainable using the scattered sub-sum ($\omega_i+\frac{1}{2}\omega_p$) and sub-difference ($\omega_i-\frac{1}{2}\omega_p$) frequencies.These are the result of interaction of the imaging beam with the half-frequency emissions of a bubble driven hard (detected by Bohn (1957) and Esche (1952) for stable and transient cavitation respectively). The acoustically-measured size is compared with that measured by microscopy and weighing. Using equation 2, the value of the polytropic index is estimated for bubbles containing air, helium, or propane, and conclusions drawn as to the adiabaticity of the process. Finally, bubble arrays are acoustically resolved and sized.

2. Experimental

The apparatus is shown in figure 1. The experiment is performed in a water tank (25 cm x 25 cm x 50 cm) lined with acoustic absorber. A variable acoustic pump frequency was generated in the water tank using a submersed 85 mm Mylar cone speaker (Radio Supplies type 248-325) linked to a signal generator (Brookdeal type 471) via a paralleled amplifier (Quad type 405-2). The amplified voltages applied to the speaker were kept constant for each separate bubble, but varied between 1.00 V_{rms} and 5.23 V_{rms} for different sizes of bubble in order to obtain a large scattered signal. A Therasonic 1030 ultrasound generator (Electro-Medical Supplies) was used to generate the 3.35 MHz continuous-wave imaging signal at 0.05 Wcm^{-2}. The possibility of drift in the frequency of signal generated by the Therasonic 1030 introducing a systematic error in the sizing was avoided by

Figure 1 Apparatus

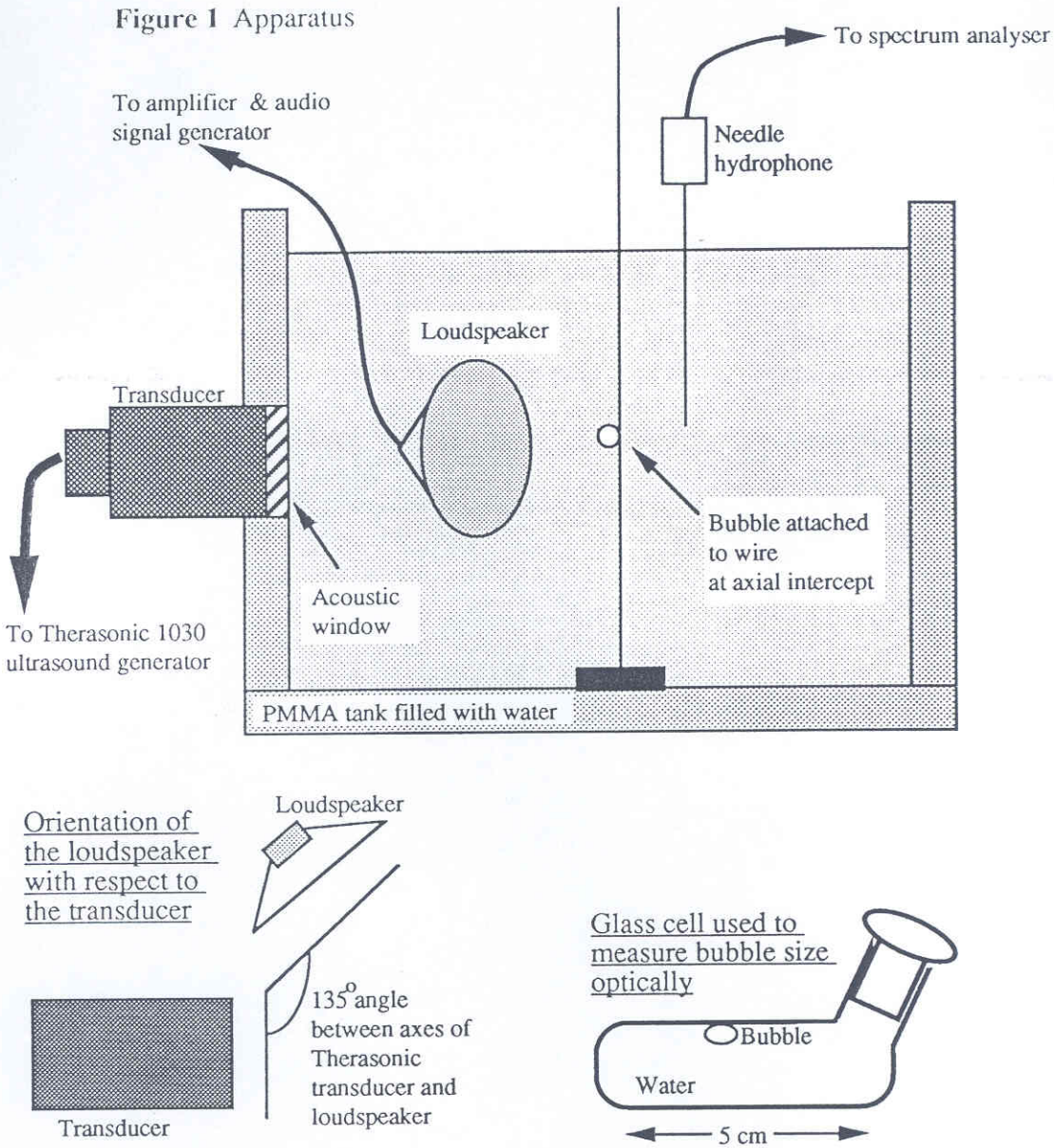

Figure 2 A typical output from the spectrum analyser. The central peak (labelled I) corresponds to the 3.35 MHz imaging signal. On either side of this are the $(\omega_i + \omega_p/2)$ and the $(\omega_i - \omega_p/2)$ signals. The two outer peaks are at the $(\omega_i + \omega_p)$ and the $(\omega_i - \omega_p)$ frequencies. The pump frequency was 3.960 kHz.

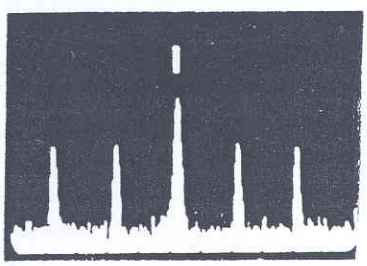

measuring the pump frequency directly using a frequency counter. The ultrasound transducer was coupled to an acoustic window in the polymethylmethacrylate (PMMA) tank. The speaker and the transducer were angled at 135° in the same horizontal plane as this prevented direct coupling between them. At the intersection of their axes, a wire (of diameter 0.5 mm) was placed. The bubble was introduced onto the wire by means of a drawn glass pipette, adhering to the paraffin wax with which the wire had been coated. A control experiment showed that this apparatus did not scatter sound non-linearly in the absence of a bubble.

A needle hydrophone (Dapco NP10-3) detected the scattered acoustic signal which was processed in a Spectrum Analyser (Marconi Instruments type TF 2370). A calibration procedure (using standard acoustic signals of known frequency and pressure amplitude) allowed the output of the Spectrum Analyser to be expressed in terms of the acoustic pressure. An example of the Analyser output can be seen in figure 2. In addition to the combination frequencies of the imaging frequency with the pump and with the subharmonic, combinations involving superharmonics were also detected. Though these were often sharper resonances, their smaller amplitude made them less suitable for sizing purposes.

For each setting of the pump frequency, the Spectrum Analyser swept across the whole of the monitored frequency range.The active element of the needle hydrophone was 10 mm radially away from the bubble, and at the same height. The hydrophone had been calibrated for this directional mode.

After the acoustic measurements on a bubble had been complete, the bubble was dislodged from the wire and captured in a glass flask (shown in figure 1). While buoyancy held it against the flat upper surface of the flask, the diameters of the bubble were measured from above and the side by a travelling microscope. Since the bubble were distorted from the spherical, an equivalent radius (R_e), equal to $^1/3$ diameter + $^1/6$ depth, was used as a useful estimate of the radius which that volume of gas would have if spherical. The error assigned to the equivalent radius reflects the use of the vernier scale on the travelling microscope. How well R_e reflects the true radius the bubble would assume if spherical (R_t) is dependent on the bubble shape in the flask.

A second method of finding the radius of the bubble if it were spherical was tried, but found to be less accurate. Here the bubble was trapped within a density bottle. The mass of the bottle and contents was then less by the volume of water displaced by the bubble, and so the bubble volume was found. The errors in the subsequent calculated R_t would be a third of the percentage error in the volume measurement. Even so, the accuracy could not compare with that involved in either the acoustic or optical measurements (which measure R_t and R_e respectively).

The series of experiments are as follows. Firstly resonance curves were measured for a series of air bubbles to determine the width of the response, and therefore the likely use of the technique in sizing, for both the ($\omega_i \pm \omega_p$) and the ($\omega_i \pm \frac{1}{2}\omega_p$) frequencies. The magnitude of the response at each set value of the pump frequency was taken as the average value of the sum and the difference pressures (though as can be seen from figure 2, the asymmetry is small). The response was plotted for both increasing and decreasing values of the pump frequency, to check that dissolution or coalescence of the bubble had not altered its resonance properties. The increment of the pump frequency was 20 Hz. To save time, a rough idea of the resonance frequency was obtained by watching the bubble as the pump frequency was quickly swept through the kilohertz range. The surface of the bubble shimmered (due to ripples on its surface, as imaged in figure 13) as the insonating frequency approached resonance. This gave a rough idea of the region of resonance, which could then be probed more accurately through pure acoustic means. This was done for five bubbles, with radii ranging from 0.65 mm to 1.035 mm. For each bubble, the pump was swept through resonance, and the magnitude of the scattered frequencies measured, until the latter

consistently remained at the level of the noise. When subsequently plotted on resonance curves, plotting ceased after the point where the signal first reaches the noise level, before remaining there.

The resonances of other bubbles (ranging in radius from 0.58 mm to 1.152 mm) were found by incrementing in pump frequency steps of 100 Hz. Though decreasing the resolution, this made the experiment more time efficient, and the results were suitable for analysis of the general trend in the polytropic index of air. The same procedure was followed for bubbles containing propane ($1<\kappa<1.13$) and helium ($1<\kappa<1.63$). Propane was used since the small range in its polytropic index reduced the uncertainty resulting from not knowing κ, and so allowed the accuracy of the other aspects of the theory to be tested. Helium was used since the wide range in possible values for κ would make the extent of the adiabaticity of the process very clear.

An attempt was made at the resolution of several bubbles simultaneously within the tank. Two bubble arrays were placed in the geometry shown in figure 3, and the pump signal swept in increments of 30 Hz to 50 Hz (depending on requirement). Finally, the bubble on the wire was photograpned at 6000 frames per second (f.p.s.) using a Hadland Hyspeed camera.

Figure 3 The geometry of the bubble arrays.

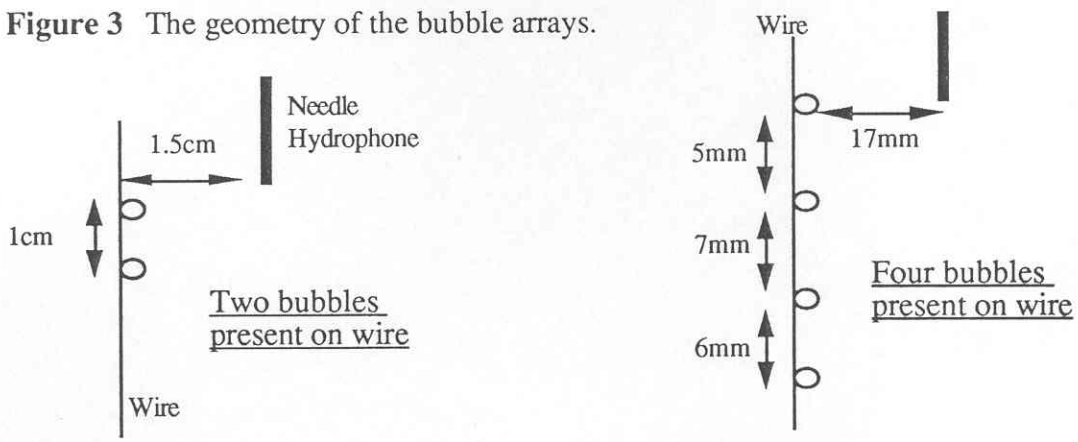

3. Results

In figures 4 and 5, part *a* corresponds to increasing the pump frequency, whilst part *b* was subsequently taken for decreasing the pump frequency. Figure 4 shows the resonance curve of a bubble. The $(\omega_i \pm \frac{1}{2}\omega_p)$ response is far sharper than the $(\omega_i \pm \omega_p)$ response, the two being plotted together for comparison. The optically measured R_e for this bubble was 0.645±0.005 mm.

A second air bubble is shown in figure 5. Again the $(\omega_i \pm \frac{1}{2}\omega_p)$ scatter tends to be sharper, though more so for increasing pump frequency (figure 5a) than for decreasing (figure 5b). An attempt to find the bubble size by weighing proved too inaccurate for comparison with acoustic sizing. Error bars are shown for the $(\omega_i \pm \frac{1}{2}\omega_p)$ data. The error represents the asymmetry of the $(\omega_i + \frac{1}{2}\omega_p)$ and the $(\omega_i - \frac{1}{2}\omega_p)$ peaks. Although error was taken for all measurements, it is not shown on figure 4 or figures 9 to 12 for clarity. The logarithmic nature of the Analyser output means the error tends to decrease the smaller the absolute value of the reading.

Some resonance scans showed a single peak for increasing pump frequency but a double peak for decreasing frequency, one peak of the doublet being at the original frequency and one at a smaller frequency. This was the result of the bubble coalescing with neighbouring bubbles that

Figure 4 The response curve of an air bubble, taken for **a)** increasing, and **b)** decreasing, values for the pump frequency. The resonance occurs at 4.90±0.02 kHz. The optically-measured equivalent radius was 0.645±0.005 mm; the atmospheric pressure, 0.1000 MPa; the water density, 1021.5 kg/m^3.

Figure 4a

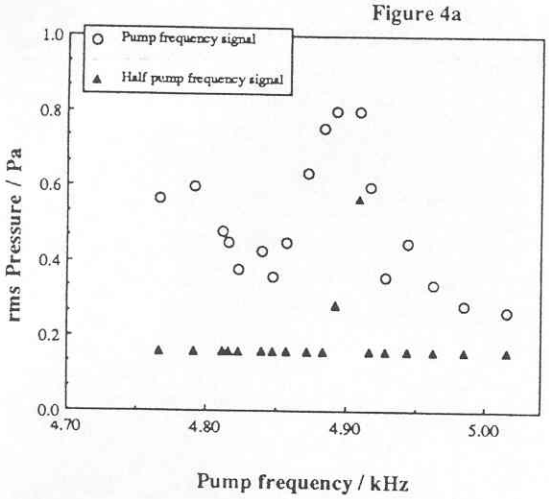

Figure 4b

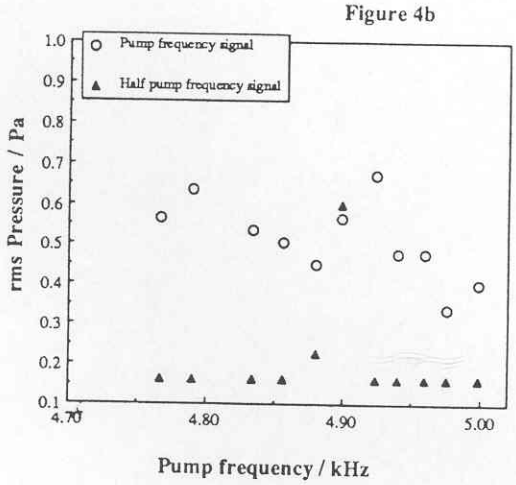

Figure 5 The response curve of an air bubble in water, taken for **a)** increasing, and **b)** decreasing, values for the pump frequency. No direct accurate estimate of the bubble size could be taken for comparison. Error bars are shown for the ($\omega_i \pm \omega_p/2$) data.

Figure 5a

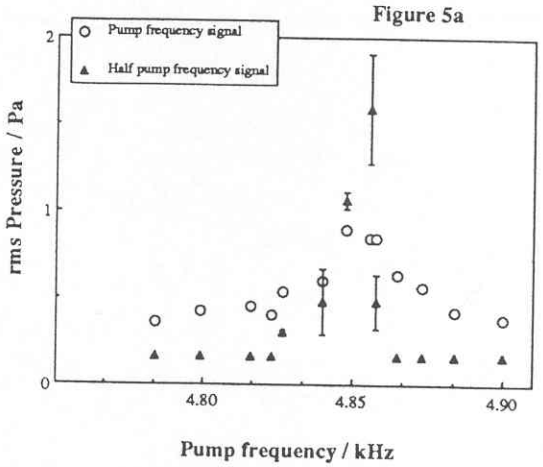

Figure 5b

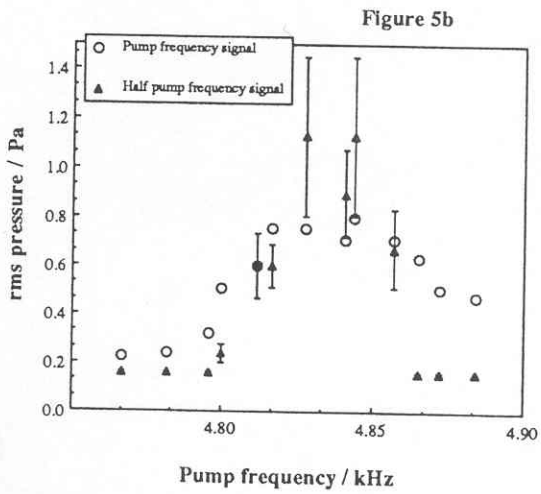

Figure 6 Resonance frequency as a function of the equivalent radius of air bubbles, compared with the theoretical estimates from equation 2.

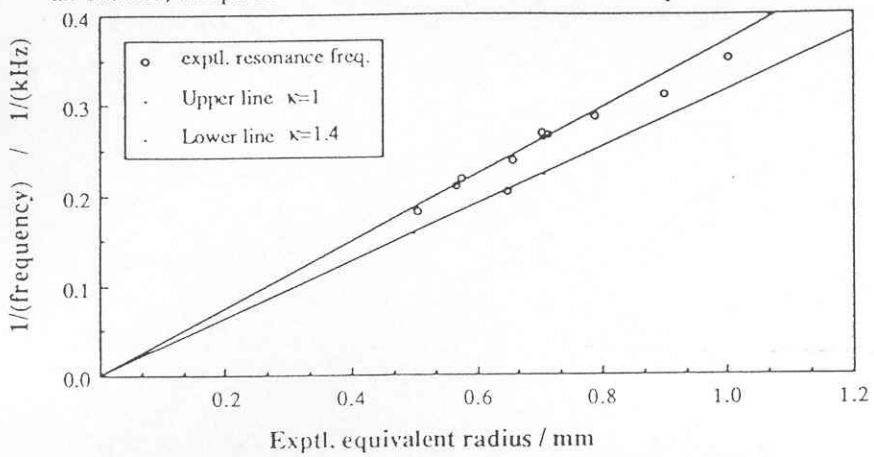

Figure 7 Resonance frequency as a function of the equivalent radius of helium bubbles, compared with the theoretical estimates from equation 2.

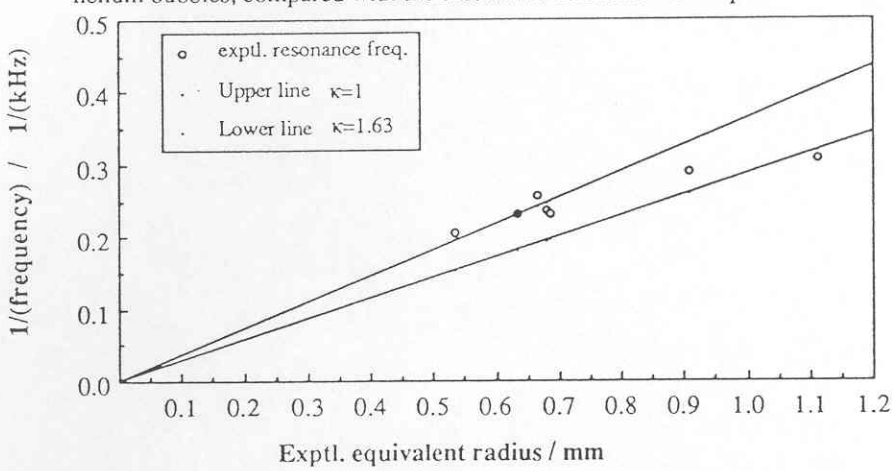

Figure 8 Resonance frequency as a function of the equivalent radius of propane bubbles, compared with the theoretical estimates from equation 2.

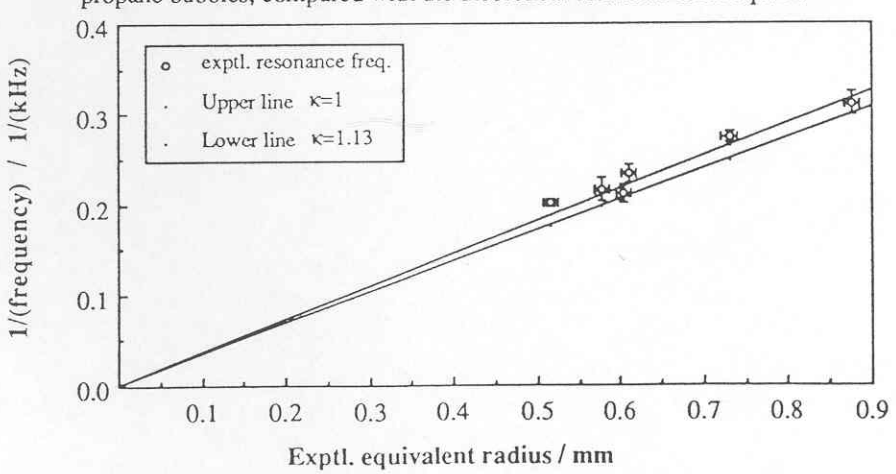

Figure 9 The response of a two-bubble array. The bubble with resonance at 4.119 kHz had an optically-measured Re of 0.662±0.005 mm. Atmospheric pressure was 0.1024 MPa, water density 1021.5 kg/m^3

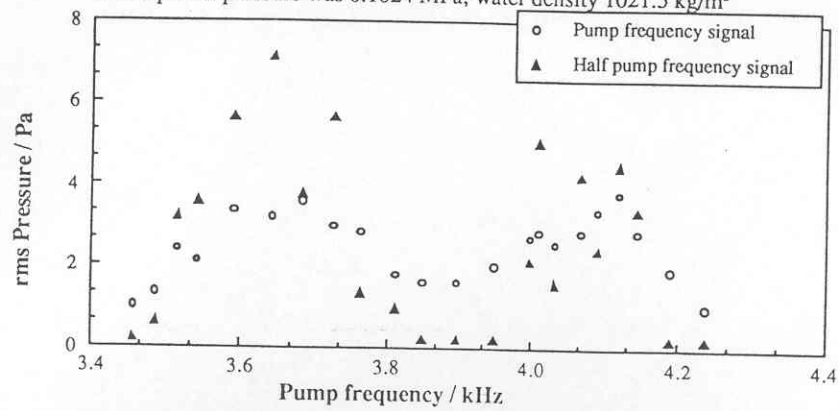

Figure 10 The reponse curve for a two-bubble array.

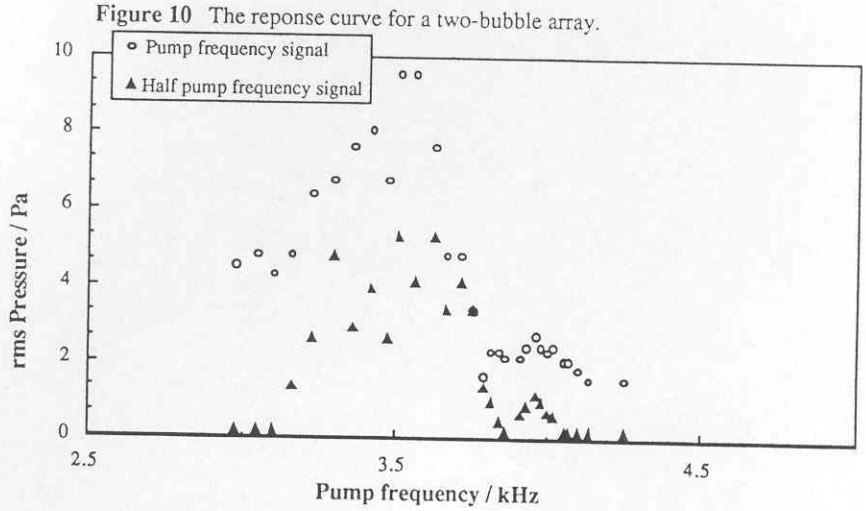

Figure 11 The acoustic response of a two-bubble array.

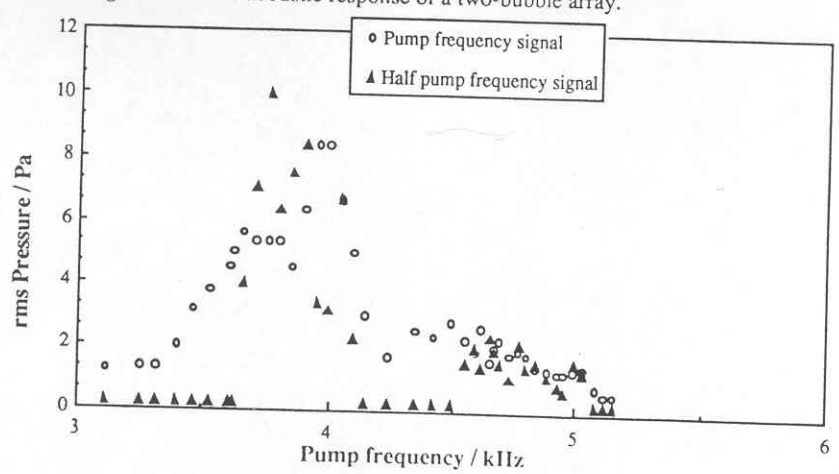

Figure 12 The acoustic response of a four-bubble array. The resonance peaks (at 4.990 kHz, 4.654 kHz, 4.384 kHz and 3.597 kHz) are arrowed. The 4.990 kHz bubble was optically measured to have $R_e = 0.481 \pm 0.005$ mm. Atmospheric pressure = 0.1026 MPa; water density = 1021.4 kg/m^3

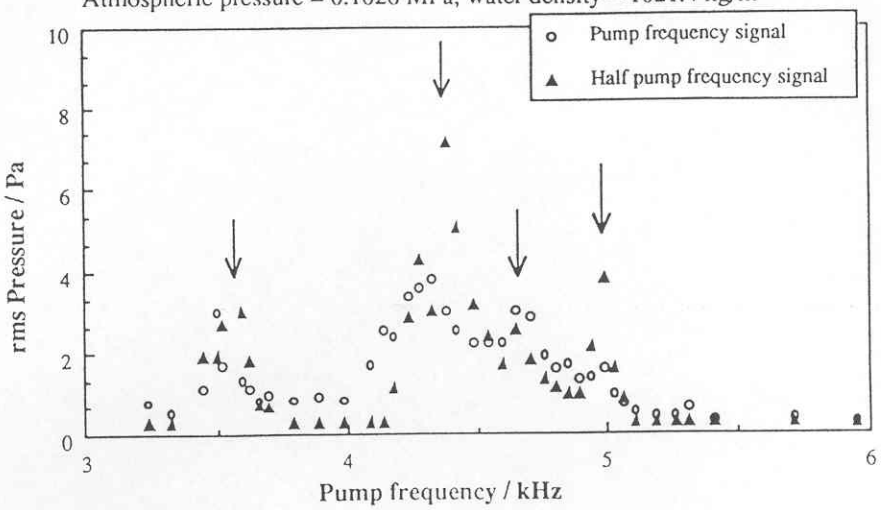

Figure 13 A selection of 9 consecutive frames, shot at 6000 fps, showing a resonating air bubble on a wire undergoing forced oscillations. The pump frequency was 4.370 kHz.

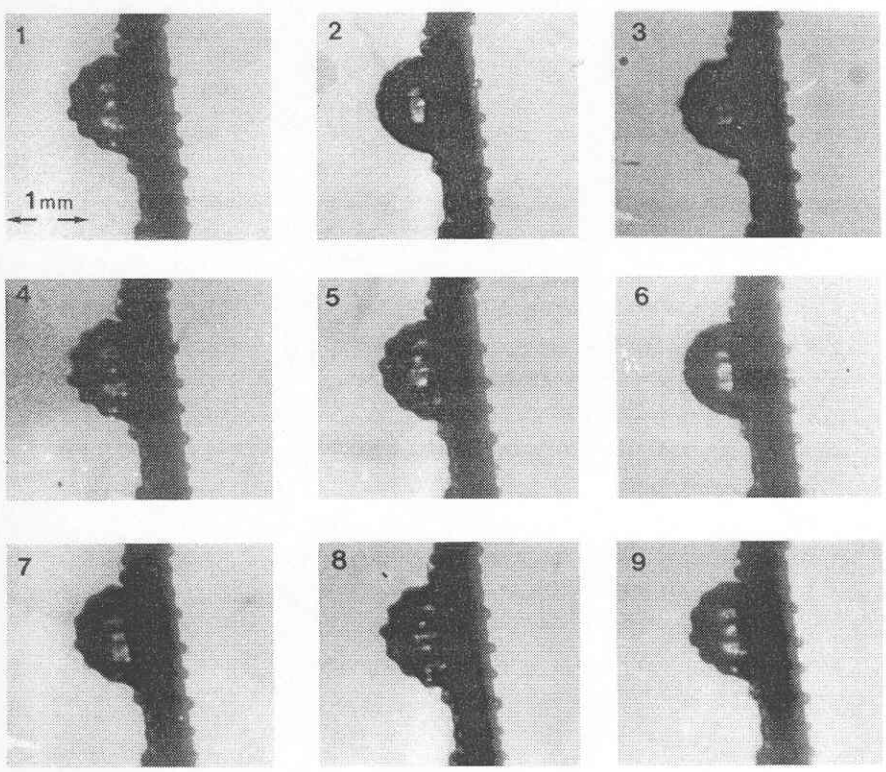

have grown out of solution and are attached to the wire (these can be seen in figure 13). Coalescence occurs as the bubble is most active, that is, when the pump frequency is passing through resonance. The absorption of the smaller bubble reduces the resonance frequency of the bubble on the wire, and so the second peak occurs. This phenomena can only be seen when the pump frequency is being reduced, since only then are the frequencies lower than the original resonance investigated after that resonance has passed.

The data from such resonance curves are used to test equation 2, and to investigate the behaviour of the polytropic index, for air (figure 6), helium (figure 7) and propane (figure 8). The error in figures 6 and 7 is smaller than the size of the point marker symbol.The reciprocal of the bubble resonant frequency, as found from the centre of the resonance curves, is plotted against the optically measured R_e. Plotted with the data points are the lines predicted by equation 2, corresponding to $\kappa=1$ (isothermal) and $\kappa=\gamma$ (adiabatic). Intermediate behaviour will correspond to the data falling graphically between these limits.

Bubble arrays are acoustically resolved in figures 9 to 12. Figures 9 to 11 show the response of three arrays, each containing two bubbles separated by 10 mm. In each case, two peaks are clearly visible, corresponding to the resonances of the bubbles. Figure 12 shows a response curve for a system of four bubbles in a line with the spacing as illustrated in figure 3. Four peaks are visible and are indicated by arrows. Each peak corresponds to the resonance of a single bubble.

Figure 13 is a selection of nine consecutive frames from a film taken at 6000 f.p.s., for a pump frequency of 4.370 kHz.

4. Discussion

The resonance curves indicate that the scattered ($\omega_i \pm \frac{1}{2}\omega_p$) signal tends to be sharper than the ($\omega_i \pm \omega_p$) signal. In this experiment the maximum is usually greater for ($\omega_i \pm \frac{1}{2}\omega_p$) than for ($\omega_i \pm \omega_p$), and on average the half-height width is 2.5±1.3 times less. As a result, the ($\omega_i \pm \frac{1}{2}\omega_p$) signal is more accurate for obtaining the resonant frequency of the bubble, with error between 0.5% and 2%. This will be the error in the radius that the bubble would have if spherical, R_t, as found from the resonance frequency using equation 2. This is more accurate than the optical or weighing methods. The sub-sum scattering would be expected to be sharper, since it is a second order effect, and so would fall off as one moves away from resonance faster than does the sum and difference scattering.

Figures 6 to 8 allow the value of κ for this process to be estimated. Best fit lines to the data gives values for κ of 1.05±0.04 for air; 0.995±0.034 for propane; and 1.15±0.11 for helium. All therefore tend towards the isothermal. Out of the twenty-three individual bubble resonances measured for the various gases, only two were found to correspond closely to the adiabatic case. All but one of the rest of the values of κ (polytropic index) lay below $1+\frac{1}{4}\gamma$ (one at $1+\frac{1}{2}\gamma$), with γ being the adiabatic ratio. Thus the process of forced oscillation can be said to be more than 75% isothermal.

The thermal diffusion length for a bubble in water is given by $\sqrt{(D_t t)}$ as found by Fujikawa and Akamatsu (1985). With $D_t=1.43\times10^{-7}$, and $t=5\times10^{-4}$ (from $\frac{1}{2}\upsilon_p = 2$ kHz), the diffusion length is 8.5 μm. The high speed photography shows the amplitude of the oscillations of the bubble to approximately 50 μm, which is of the same order of magnitude as the thermal diffusion length. This suggests that heat transfer is possible during the oscillation, and hence this process could be isothermal. The photographs also show oscillations of the bubble wall with frequency of 2.28±0.11 kHz, showing that the half pump frequency oscillations are present (since the framing

rate does not satisfy the Nyquist criterion, this was measured independently at regions of the film corresponding to 5000, 6000 and 7000 f.p.s.). Since the observed ripples can be expressed as a summation of spherical harmonics, there will be various frequencies present in the bubble wall oscillation.

Benjamin and Ursell (1954) investigated the waves on the free surface of a vertically-vibrated cylinder of liquid. These waves were at half the exciting frequency, a phenomenon first recognised by Faraday (1831). Neppiras (1969) suggested that such Faraday waves on the surface of bubbles are generated at half the excitation frequency, and investigated the possibility that these surface oscillations might be responsible for subharmonic emissions. He concluded that a more likely source is the emission from bubbles, at their own resonances, when they are insonated with a frequency f_o twice that of their resonance. However in the current experiment bubbles are insonated at their resonant frequency, and the subharmonic at half that frequency is still detected. Thus surface waves seem a more likely source. In fact, Neppiras (1969) concludes: "Although it has never been found possible to relate subharmonic signals with surface-wave activity on the bubbles, surface waves would be expected to contribute to the $f_o/2$ signals-the possibility is not yet ruled out." Neppiras suggests that the surface oscillations, involving as they do no change in volume, would not be able to couple strongly with low-viscosity liquids, thereby reducing their acoustic emission. However, more recent work by Longuet-Higgins (1989), using nonlinear analysis, suggests that oscillations not involving a volume change might nevertheless contribute to the sound signal. Therefore it is still not known what contribution is made to the subharmonic by the surface mode, and what is simply the result of an nonlinear oscillator driven hard.

Multibubble arrays could be acoustically resolved. Attempts to correlate the acoustically-measured bubble size (giving R_t)with optical measurements of R_e were not always successful, as the bubbles sometimes escaped. The bubbles for the resonance curves in figures 10 and 11 were not captured, and only one of the bubbles was captured for figure 9. Figure 9 shows two peaks at 4.119 kHz and at 3.644 kHz.This corresponds to approximate radii of 0.68 mm and 0.77 mm, with the difference being 90 μm. Figure 10 has peaks at 3.506 kHz and 3.956 kHz, corresponding to approximate radii of 0.80 mm and 0.71 mm, again with a difference of 90 μm. Figure 11 has peaks at 3.90 kHz and 4.76 kHz, which corresponds to radii of 0.72 mm and 0.59 mm. This shows that bubbles of radii differing by 90 μm can be differentiated between if their resonance frequencies are in the region of 3-5 kHz. This represents resolution at about 12% of the radii.The bubble with a resonance frequency of 4.119 kHz in Figure 9 was optically measured to have an equivalent radius of 0.662 mm, corresponding well to those observed resonance frequency.

For the four-bubble array shown in figure 10, only one of the bubbles was captured. It was optically measured to have R_e=0.555±0.005 mm, corresponding to the bubble that was seen to resonate at 4.99±0.01 kHz. This bubble disintegrated slightly when removed from the wire. This resonance frequency corresponds to a bubble radius R_t of 0.57±0.05 mm (using κ = 1.049). The peaks at 4.654 kHz and 4.384 kHz correspond to bubble radii of 0.61 mm and 0.64 mm respectively, indicating that this system is capable of resolving bubbles differing in radius by only 30 μm. This represents the resolution of two bubbles whose radii differ by 5%.

5. Conclusions

The insonification of a bubble with an audio pump signal, ω_p, and a megahertz imaging signal, ω_i, produces scattered signals that can be used as an accurate bubble sizing method. The method is

more accurate when the signals at $(\omega_i \pm \frac{1}{2}\omega_p)$ are observed, as opposed to those at $(\omega_i \pm \omega_p)$. The bubble radius can be obtained using the $(\omega_i \pm \frac{1}{2}\omega_p)$ signals to an accuracy greater than that available by optical or weighing methods for bubbles with resonance frequencies of the order 3 kHz. In addition, the value given reflects the true radius the bubble would assume if spherical (R_t), despite its actual shape, so facilitating any subsequent volumetric and acoustic analyses.

The sum and difference sizing method has been able to distinguish between two bubbles, a distance of 5 mm apart, differing in radius by about 5%. This was observed to give a difference in resonance frequency of 270 Hz with the resonance frequencies being of the order of 4 kHz. Knowledge of the polytropic index, which in this study tends to the isothermal case, will improve the accuracy of this method of acoustic sizing.

6. Acknowledgements

TGL wishes to thank Magdalene College, Cambridge, and the Science and Engineering Research Council, for Research Fellowships. The authors wish to thank K. Fagan for his help with the photography, and Marconi Underwater Systems Ltd. for a grant to the laboratory.

7. References

Belcher, E.O. (1980) 'Quantification of bubbles formed in animals and man during decompression.' IEEE Trans. Biomed. Eng., 27, 330-338.

Benjamin, T.B. and Ursell, F. (1954) 'The stability of the plane free surface of a liquid in vertical periodic motion,' Proc. Roy. Soc. (London), A225, 505-515.

Bohn, L. (1957) 'Acoustic pressure variation and the spectrum in oscillatory cavitation,' Acustica, 7, 201-216.

Esche, R. (1952) 'Untersuchung der schwingungskavitation in flüssigkeiten,' Acustica, 2, AB208-AB218.

Fairbank, W.M. and Scully, M.O. (1977) 'A new noninvasive technique for cardiac pressure measurement; resonant scattering of ultrasound from bubbles,' IEEE Trans. Biomed. Eng., 24, 107-110.

Faraday, M. (1831) 'On the forms and states assumed by fluids in contact with vibrating elastic surfaces,' Phil. Trans., 319-340.

Fujikawa, S. and Akamatsu, T. (1985) 'Effects of heat and mass transfer on the impulsive pressure developed by the bubble collapse,' Bull. JSME., 28, 267-273.

Gross, D.R., Miller, D.L. and Williams, A.R. (1985) 'A search for ultrasonic cavitation within the canine cardiovascular system,' Ultrasound in Med. Biol., 11, 85-97.

Hulshof, H.J.M. and Schurink, F. (1985) 'Continuous ultrasonic waves to detect steam bubbles in water under high pressure,' Kema Scientific and Technical Reports, 3, 61-69.

Kisman, H. (1977) 'Spectral analysis of Doppler ultrasonic decompression data,' Ultrasonics, 15, 105-110.

Leighton, T.G. and Walton, A.J. (1987) 'An experimental study of the sound emitted from gas bubbles in a liquid,' Eur. J. Phys., 8, 98-104.

Longuet-Higgins, M.S. (1989) "Monopole emission of sound by asymmetric bubble oscillations. Part 1. Normal modes,' J. Fluid Mech., 201, 525-541.

Main, I.G. (1984) Vibrations and Waves in Physics (2nd edition), Cambridge University Press, Cambridge. pp 104-107.

Miller, D.L. (1981) "Ultrasonic detection of resonant cavitation bubbles in a flow tube by their second-harmonic emissions,' Ultrasonics, 19, 217-224.

Miller, D.L., Williams, A.R. and Gross, D.R. (1984) 'Characterization of cavitation in a flow-through exposure chamber by means of a resonant bubble detector,' Ultrasonics, 22, 224-230.

Minnaert, M. (1933) "On musical air-bubbles and sounds of running water,' Phil. Mag., 16, 235-248.

Neppiras, E.A. (1969) 'Subharmonic and other low-frequency emissions from bubbles in sound-irradiated liquids,' J. Acoust. Soc. Am., 46, 587-601.

Neppiras, E.A. (1980) 'Acoustic cavitation,' Phys. Rep., 61, 159-251.

Newhouse, V.L. and Shankar, P.M. (1984) 'Bubble size measurement using the nonlinear mixing of two frequencies,' J. Acoust. Soc. Am., 75, 1473-1477.

Nishi, R.Y. (1972) 'Ultrasonic detection of bubbles with Doppler flow transducers,' Ultrasonics, 10, 173-179.

Pumphrey, H.C. and Crum, LA. (1989) "Sources of ambient noise in the ocean," Technical Report for Office of Naval Research (USA), Ocean Acoustics Division, Contract No. N0014-87-K-0019, May 1989.

Pumphrey, H.C. and Walton, A.J. (1988) 'Experimental study of the sound emitted by water drops impacting on a water surface,' Eur. J. Phys., 9, 225-231.

Shankar, P.M., Chapelon, J.Y. and Newhouse, V.L. (1986) 'Fluid pressure measurement using bubbles insonified by two frequencies,' Ultrasonics, 24, 333-336.

Tickner, E.G. (1982) 'Precision microbubbles for right side intercardiac pressure and flow measurements,' in Meltzer, R.S. and Roeland, J. (eds.), Contrast Echocardiography, (Nijhoff, London, 1982).

Walton, A.J. and Reynolds, G.T. (1984) 'Sonoluminescence,' Advances in Physics, 33, 595-660.

Watkins, R.D., Barret, L.M. and McKnight, J.A. (1988) "Ultrasonic waveguide for use in the sodium coolant of fast reactors,' Nucl. Energy, 27, 85-89.